

# Structure of low-lying $^{12}\text{C}$ -resonances

R. Álvarez-Rodríguez<sup>1</sup>, E. Garrido<sup>2</sup>, A.S. Jensen<sup>1</sup>, D.V. Fedorov<sup>1</sup>, and H.O.U. Fynbo<sup>1</sup>

<sup>1</sup> Institut for Fysik og Astronomi, Aarhus Universitet, DK-8000 Aarhus C, Denmark

<sup>2</sup> Instituto de Estructura de la Materia. Consejo Superior de Investigaciones Científicas.  
Serrano 123, E-28006 Madrid, Spain

Received: date / Revised version: date

**Abstract.** The hyperspherical adiabatic expansion is combined with complex scaling and used to calculate low-lying nuclear resonances of  $^{12}\text{C}$  in the  $3\alpha$ -model. We use Ali-Bodmer potentials and compare results for other potentials  $\alpha - \alpha$  with similar  $^8\text{Be}$ -properties. A three-body potential is used to adjust the  $^{12}\text{C}$ -resonance positions to desired values extending the applicability of the method to many-body systems decaying into three  $\alpha$ -particles. For natural choices of three-body potentials we find 14 resonances below the proton separation threshold, i.e. two  $0^+$ , three  $2^+$ , two  $4^+$ , one of each of  $1^\pm$ ,  $2^-$ ,  $3^\pm$ ,  $4^-$ , and  $6^+$ . The partial wave decomposition of each resonance is calculated as function of hyperradius. Strong variation is found from small to large distance. Connection to previous experimental and theoretical results are discussed and agreements as well as disagreements are emphasized.

**PACS.** 21.45.+v Few-body systems – 21.60.Gx Cluster models – 25.70.Ef Resonances – 27.20.+n. 6 <= A <= 19

## 1 Introduction

The low-lying nuclear bound states and resonances of  $^{12}\text{C}$  have been the subject of numerous investigations. Surprisingly a number of issues are still not settled, e.g. what are the energies of the low-lying resonances below the proton separation threshold 15.96 MeV of excitation energy, what are their angular momenta, their structure in general, and their decay properties. Substantial experimental efforts are presently devoted to find answers to these questions [1]. This is partly motivated by the interest from astrophysics [2], but the research has basic intrinsic interest in its own right.

Experiments often focus on specific properties and/or specific resonances, but taken together more and more accurate data accumulate [3]. Open questions remain on  $0^+$  and  $2^+$  resonances [4] above the first  $0^+$  resonance at 7.6 MeV, e.g. in [3] there are only tentatively assigned candidates. Recently this has been addressed experimentally both by inelastic scattering of alpha-particles on  $^{12}\text{C}$  [5, 6], and by studies of the beta-decays of  $^{12}\text{N}$  and  $^{12}\text{B}$  [7]. These studies are in reasonable agreement on the existence of a broad  $0^+$  state near 10 MeV, but give three different suggestions for the position and width of the first  $2^+$  resonance.

The accurate measurements and the related careful analysis call for a reliable theoretical description. The theoretical efforts go back at least fifty years but consensus has not been reached. Advanced recent attempts can be divided into microscopic models dealing either directly

with an unbiased 12-body nuclear problem or with various cluster constraints of four nucleons within each of the three  $\alpha$ -particles. Within the first group we find the no-core shell model [8], the stochastic variational method [9] and Greens function Monte Carlo calculations [10]. None of these methods have so far been able to provide satisfactory answers to the present continuum problem. In the second group we find antisymmetric molecular dynamics [11], Fermionic molecular dynamics [12], and resonating group methods [13]. These methods are very ambitious as well but more directed to account for possible cluster structures. However, they have also not provided convincing answers as for example evidenced by mutual disagreements. Furthermore, the same tendency of concentrating on specific properties and resonances is seen as in the experimental studies. Systematic investigations of all low-lying resonances with a given model are very few [15, 16, 14, 11], and not easily reconciled with the newest experimental information.

These microscopic theories have so far not provided energy distributions of the  $\alpha$ -particles after decay of the resonances. These observables are difficult to compute with a reasonable accuracy, but nevertheless this is precisely where the accurate and complete experimental information accumulates [7]. To address these problems we scale down the ambitions to a practical yet challenging size where systematic investigations are possible.  $-3\alpha$  cluster models suggest themselves since energies below the proton separation threshold at 15.96 MeV only allow  $3\alpha$  and  $\gamma$ -emission. Many-body resonances decaying into three par-

ticles necessarily reduce to a three-body problem at large distance. The validity of  $3\alpha$  models extends for short-range interactions to surprisingly small distances where the three particles almost touch each other [17–19]. The  $\alpha$ -cluster structure may dominate and the description can possibly be extended to even smaller distances. However, detailed information at small distance can not be expected without introduction of nucleonic degrees of freedom. For this reason three- $\alpha$  models can only be expected to describe intermediate and large-distance properties related to  $\alpha$ -clustering. In particular electromagnetic transitions depend sensitively on short-distance properties of the wavefunctions and are therefore in general not reliably accessible within these models.

The limitations of these models are not established. The energy distributions after decay are large-distance properties and as such possible to compute rather accurately with few-body techniques [20]. However, even this  $3\alpha$  problem is very challenging. First because we are then dealing with a three-body quantum mechanical Coulomb problem in the continuum. Second because we want a comprehensive picture describing all resonances and all three-body observables within the same model. The second requirement is especially demanding since the resonance may vary from two-body to genuine three-body large-distance structures. Coulomb and short-range interactions must then be treated on an equal footing. However, the techniques and methods are available and recently applied in similar practical three-body computations [21].

We shall use the hyperspherical adiabatic expansion method [22] combined with complex scaling of the coordinates [19]. This method restricts the applications to resonances where the width is relatively small compared to the real part of the energy. In any case as these states are closest to the real axis they have the strongest direct influence on observables. Furthermore, as obtained by analytical continuation they have the smallest uncertainty due to the choice of parametrization of the interactions. To describe properly the different types of asymptotic large-distance structures we use the Faddeev decomposition. Then the individual components can simultaneously account for several two-body substructures like narrow resonances in corresponding subsystems. This is a tremendous advantage over one-component methods.

The purpose of the present work is to (i) establish that the  $3\alpha$ -cluster model can answer questions related to properties of many-body resonances, (ii) give a survey of the structures of possible  $^{12}\text{C}$ -resonances below the excitation energy of 15.96 MeV, and (iii) lay out the foundation for calculations of energy distributions after decay. We shall build on experience gained from three-body investigations of bound states and continuum properties of  $^6\text{He}$  [23],  $^{11}\text{Li}$  [25, 24, 20],  $^{17}\text{Ne}$  [26],  $^6\text{Be}$  and  $^6\text{Li}$  [27] as well as more general investigation of three-body resonance properties [28–30]. In section 2 we shall first give a brief sketch of the theoretical formulation. In section 3 we discuss the resonances and their structures for a specific two-body interaction. In section 4 we describe the sensitivity to in-

teractions. Finally section 5 contains a summary and the conclusions.

## 2 Basic theoretical ingredients

We use techniques described in details in previous publications. It suffices here to give a brief sketch of the procedure employed in the present work. The general framework can be found in [22]. The new results found for  $^{12}\text{C}$  will be discussed in more details in the following sections. The adiabatic hyperspherical expansion method with the Faddeev decomposition is well established in applications to nuclear three-body systems [25]. The combination with complex rotation to compute resonances is also known to be very efficient for these systems [19]. The method consists of a number of steps: First we define the coordinates where the hyperradius  $\rho$  is the most important, i.e.

$$\rho^2 = \frac{4}{3} \sum_{i<j}^3 (\mathbf{r}_i - \mathbf{r}_j)^2 = 4 \sum_{i=1}^3 (\mathbf{r}_i - \mathbf{R})^2, \quad (1)$$

where  $\mathbf{r}_i$  is the coordinate of the  $\alpha$ -particle number  $i$  and  $\mathbf{R}$  is the center-of-mass coordinate of  $^{12}\text{C}$ . The factor of 4 is arbitrary and chosen to correspond to a normalization mass equal to that of the nucleon. The remaining relative coordinates are all dimensionless angles.

Second we choose a two-body interaction as input for the angular part of the complex rotated Faddeev equations. This interaction should reproduce the low-energy scattering properties of all pairs of particles in the three-body system. A smaller amount of data like scattering length and effective range may also be sufficient, or perhaps the low-lying two-body resonance energies and their widths. We use the Ali-Bodmer potentials [31] in various combinations, and sometimes compared with results from even simpler interactions adjusted to reproduce selected  $^8\text{Be}$ -properties. The hyperradius is fixed and the solutions to the angular wavefunction  $\Phi_n$  are calculated.

Third a three-body Gaussian potential,  $V_{3b} = S \exp(-\rho^2/b^2)$ , is selected. Such potentials are necessary to reproduce accurately few-nucleon observables [32]. We choose  $b \approx 6$  fm such that  $\rho = b$  corresponds to three touching  $\alpha$ -particles. This three-body potential is diagonal, i.e. added to each of the adiabatic potentials whereas we assume that the corresponding three-body couplings are zero. This construction maintains the structure of a three-body state, but by varying the strength the energy position can be adjusted to reproduce the measured value for each resonance.

An individual adjustment is crucial in a comparison of partial widths which depend exponentially on the energy due to barrier penetration. Since the small-distance structure easily can vary from state to state the three-body potential should in principle be state-dependent. However, we choose the same potential for all states of given angular momentum and parity,  $J^\pi$ . One simple reason is that this essentially corresponds to the number of known experimental data and we can then estimate or predict the positions and widths of other states with the same  $J^\pi$ .

States with different  $J^\pi$  can be expected to differ more in structure and thus require different three-body potentials. We choose to ignore the two bound states because they, and especially the ground state, have a smaller size and their structure can then be expected to involve more nucleonic (less  $\alpha$ -cluster) degrees of freedom. Although it is possible to construct a three-body potential which reproduces energies of both the ground state and the lowest  $0^+$  resonance [33, 34] it is uninteresting in the present context since the important intermediate and large distance-structure would remain unchanged.

Fourth we find the radial wavefunctions,  $f_n(\rho)$ , by solving the coupled set of radial equations arising from expansion of the total wavefunction  $\Psi$  on  $\Phi_n$ , i.e.

$$\Psi^{(JM)} = \frac{1}{\rho^{5/2}} \sum_n f_n(\rho) \Phi_n^{(JM)}(\rho, \Omega). \quad (2)$$

The expansion coefficients  $f_n(\rho)$  are exponentially decaying for resonances when the rotation angle  $\theta$  of the hyperradius is larger than corresponding to the three-body resonance. Then both real and imaginary parts,  $E_0 = E_R - iE_I$ , of the resonance energy,  $E_0$ , are determined by  $f_n(\rho \rightarrow \infty) = C_n \exp(+i\kappa\rho)$  with  $\kappa = \sqrt{2mE_0/\hbar^2}$ .

In principle some of the channels could correspond to two-body bound states or narrow resonances which asymptotically would have radial wavefunctions decaying with a wave number corresponding to the three-body energy minus that tied up in the two-body system. In practice this only has marginal importance since the radial wavefunction in any case decreases towards zero for large distances. The interpretation, and maybe the analysis, in terms of direct or sequential decay may however be very different.

Fifth the structures of the resonance wavefunctions are computed and expressed in terms of two-body partial waves. We extract the amplitudes (above called the radial wavefunctions) for each of the adiabatic potentials, and then we partial wave decompose each of these adiabatic components. The dependence on hyperradius can be substantial corresponding to a dynamical evolution of the resonance from small to large distances.

In these steps the problems with the Coulomb interaction are not mentioned although the large-distance asymptotic behavior is mathematically unknown for continuum states. We adopt the pragmatic procedure to treat the Coulomb interaction completely numerically. The general behavior and convergence properties can then be investigated and extracted if necessary [21]. Problems would reveal themselves intrinsically in the process as numerical inconsistencies.

### 3 Resonances and their structure

The sequence of resonances is computed with the Ali-Bodmer potential “AB(a’)” [31] which reproduce the  $s$ ,  $d$  and qualitatively also the  $g$ -wave  $\alpha$ - $\alpha$  phase shifts. The interactions for higher partial waves are the same as for

$g$ -waves. The  $^8\text{Be}$  resonances of  $0^+$ ,  $2^+$ ,  $4^+$  have energies ( $E_R$ ) and widths ( $\Gamma = -2E_I$ ) given by  $(E_R, \Gamma) = (100, 0.010)$  keV,  $(2.7, 1.5)$  MeV, and  $(9.7, 8.0)$  MeV, respectively. The definitions correspond to poles of the  $S$ -matrix, and should be compared to the experimental values of  $(E_R, \Gamma) = (92, 0.0068)$  keV,  $(3.1, 1.5)$  MeV, and  $(11.5, 4)$  MeV, respectively. The  $4^+$ -state is not very well reproduced although the information is derived from phase shifts reproducing the data.

#### 3.1 Partial waves

For each of the 14 resonances angular momentum and parity constrain the contributing two-body components within the three-body system. The partial wave orbital angular momenta between two particles in one Jacobi system and that of the third particle are denoted by  $\ell_x$  and  $\ell_y$ , respectively. The number of partial waves is rather small because the  $\alpha$ -particle has zero spin and the symmetry requirement eliminates in addition several components. The Faddeev components are the same in all three Jacobi systems. The number of basis states needed to describe the necessary number of partial waves can only be decided a posteriori. Accuracy is optimized by choosing large basis sets, enumerated by the hyperspherical quantum number  $K_{max}$ , when the contribution is large for a given partial wave.

Convergence has been achieved with the sets of quantum numbers shown in table 1. The large values of  $K_{max}$  should roughly be divided by two to give the corresponding number of basis states in each partial wave. This means that the total number of basis states is about  $3 \times 90$  for  $\ell_x = \ell_y = 0$ , and in total for the  $0^+$ -resonances the basis consists of about 700 states. Some of the other resonances have a larger number of basis states. With present day computers these numbers are far from being large but still extremely efficient compared to the use of only one Jacobi system and all possible partial waves consistent with one value of  $K_{max}$  [35]. These high partial waves are needed for one Jacobi system to describe configurations with two spatially close-lying particles relatively far from the third particle. The Faddeev decomposition takes care of that in the present formulation.

A given angular momentum and parity of an intended  $^{12}\text{C}$ -state needs a set of these partial wave components. However, more than one  $^{12}\text{C}$ -state with this spin and parity may be found from such a set. The probability to find each partial wave for each resonance is also given in table 1. We shall postpone the discussion of these values until section 3.4.

#### 3.2 Adiabatic potentials

The adiabatic potentials result from a full quantum mechanical solutions of the angular part of the Faddeev equation for fixed hyperradius. Each potential corresponds to a specific combination of the partial waves, in some cases

**Table 1.** Components included for each  $J^\pi$  state of  $^{12}\text{C}$ . The columns two and three give orbital angular momenta in each Jacobi system column four gives the maximum value of the hypermomentum  $K$ . In the last columns  $W_i$  give the probabilities in % for finding these component in the  $i$ -th resonance.

$J^\pi$	$\ell_x$	$\ell_y$	$K_{max}$	$W_1$	$W_2$	$W_3$
$0^+$	0	0	180	83	44	
	2	2	180	16	54	
	4	4	80	0	2	
$1^+$	2	2	180	86		
	4	4	180	14		
$2^+$	0	2	120	45	13	4
	2	0	120	45	10	45
	2	2	180	7	65	5
	2	4	80	1	0	32
	4	2	100	0	2	14
$3^+$	2	2	90	36		
	2	4	90	32		
	4	2	90	32		
$4^+$	0	4	80	27	5	
	2	2	120	39	8	
	2	4	160	2	44	
	4	0	120	27	18	
	4	2	120	4	25	
	4	4	100	0	1	
$6^+$	0	6	50	3		
	2	4	90	62		
	2	6	50	1		
	4	2	70	15		
	6	0	70	19		
$1^-$	0	1	140	30		
	2	1	180	48		
	2	3	140	22		
$2^-$	2	1	180	59		
	2	3	140	39		
	4	5	80	1		
$3^-$	0	3	140	28		
	2	1	180	65		
	2	5	100	1		
	4	1	80	5		
$4^-$	2	3	160	72		
	2	5	160	1		
	4	1	160	26		

strongly varying with  $\rho$ . These structures form the basis for the radial solution which truly is a resonance in the three-body continuum. Very few angular eigenvalues are usually needed for convergence, and their behavior are decisive for the resulting resonances. This is not a trivial conclusion, since each point of these potentials by definition corresponds to the same  $\rho$ , but different configurations are otherwise allowed. It is not obvious at all that the structures of the resonances predominantly arise from these combinations of configurations contributing to each adiabatic potential.

We show in fig. 1 the real parts of these potentials including  $V_{3b}$  corresponding to the quantum numbers of each of the resonances. The imaginary parts are small, oscillate around zero and vanish at large  $\rho$ . All these potentials di-

verge as  $\rho^{-2}$  when  $\rho \rightarrow 0$  due to the generalized centrifugal barrier. They vanish as  $1/\rho$  for large  $\rho$  where Coulomb is the only contributing interaction. At relatively small distances the potentials have minima supporting the bound states and resonances. The sizes of these pockets are larger than obtained from the two-body interaction which in most cases is far from sufficient to place the resonance at the correct energy. Therefore we added in each case a diagonal, short-range three-body potential designed to mock up effects of the intrinsic degrees of freedom in a  $3\alpha$ -model at short distances where the three  $\alpha$ -particles overlap. This allows us to stay within the three-body model and still provide the proper boundary condition at small distance at the right energy.

The three-body potentials are individually adjusted to reproduce one of the energies, but chosen to be the same for all adiabatic potentials of given angular momentum and parity. We typically choose the best known of the resonances since it is the continuum state of lowest energy, i.e. closest to the threshold for 3 free  $\alpha$ -particles. Obviously the bound states are better known but their structures can easily differ even more from the  $3\alpha$ -structure than the resonance states. The three-body potentials could then differ substantially and predictions for other resonances probably would be less accurate. The systems with wavefunctions localized outside the overlap region for the  $\alpha$ -particles should need less three-body potential and then be more reliably calculated in the  $3\alpha$ -model. For example the ground state could be a spatially confined structure while  $0^+$ -resonances could be fairly good three-body states.

For the  $0^+$ ,  $2^+$  and  $4^+$ -cases two or three minima appear in different potentials indicating the possibility of different structures of low-lying resonances. For the  $1^+$ -case the minimum only appears after addition of the three-body potential indicating that the corresponding structure at small distance differs substantially from three  $\alpha$ -particles. All negative parity states exhibit one minimum at distances larger than the 6 fm chosen as the range of the three-body interaction.

### 3.3 Resonance energies

The length coordinate,  $\rho$ , is rotated in the complex plane and the adiabatic potentials including non-diagonal terms are computed. By adding the diagonal three-body potential all quantities are specified in the coupled set of radial equations. The solutions are the three-body resonances where key quantities are real and imaginary parts of the energies. The strength of the three-body potential is used to move one bound state or one resonance into a preferred position for each set of angular momentum and parity. If there is more than one solution they are moved simultaneously by the same potential. The range of the three-body potential is kept at the same value implying that the width is predicted and not fitted. The associated uncertainties are discussed in section 4.

The computed results for the resonance energies are shown in fig. 2. The individual figures all exhibit the same

**Table 2.** Calculated and measured energies  $E_R$  (in MeV) and partial  $\alpha$ -decay widths  $\Gamma_R$  (in keV) of the resonances for different  $J^\pi$ . Since our formalism cannot describe an isospin one state, we found only one  $1^+$  resonance whose energy has been adjusted to reproduce both measured values. Experimental values (labeled “exp”) are from [3,7,1] and calculated results (labeled “th”) are obtained with the two-body interaction “AB(a’)” and the three-body interaction parameters  $S$  (in MeV) and  $b$  (in fm) given here. The energies are measured from the  $3\alpha$  threshold. The computations are for a rotation angle  $\theta$  (in rad). The  $1^+$  state at 7.84 MeV labeled  $T = 1$  has isospin one.

$J^\pi$	$E_{R,exp}$	$\Gamma_{R,exp}$	$E_{R,th}$	$\Gamma_{R,th}$	$S$	$b$	$\theta$
$0^+$	-7.25	0.0	-5.19	0.0	-20.0	6	0.1
	0.38	0.0085	0.38	0.0625	-20.0	6	0.1
	4.3	3490	3.95	1000	-20.0	6	0.1
$1^-$	3.57	315	3.61	475	-2.8	6	0.1
$3^-$	2.37	34	2.33	68	-1.7	6	0.075
$2^+$	-2.875	0.0	-3.04	0.0	-17.0	6	0.17
			1.38	132	-17.0	6	0.17
	3.88	430	4.48	1086	-17.0	6	0.17
	6.3	1700	6.49	2250	-17.0	6	0.17
$4^+$			3.25	396	-25.5	6	0.1
	6.81	258	6.83	606	-25.5	6	0.1
$6^+$			7.13	1267	-20	6	0.15
$2^-$	4.55	260	4.53	452	-2.8	6	0.1
$1^+$	5.43	0.0177	5.42	48.6	-92	6	0.1
	$T=1$ 7.84	0.0018	7.70	948	-78	6	0.1
$3^+$			7.13	1450	-20	6	0.1
$4^-$	6.08	375	5.98	1035	-1.8	6	0.15

dominant features with a series of points forming almost a straight line. Each of these points corresponds to a continuum state. These discretized three-body continuum states appear due to an imposed condition of zero radial wavefunction at the boundary of a large box. The energies appear on the straight line arising by rotation of an angle  $2\theta$  around the origin. The fluctuations are due to numerical uncertainties.

The points above the straight line are the resonance energies appearing with positive real parts,  $E_R$ , and negative imaginary parts,  $E_I = -\Gamma/2$ , where  $\Gamma$  is the width of the resonance. The radial wavefunctions of these resonances vanish exponentially at large distances corresponding to outgoing waves in all channels. This boundary condition is identical to those valid for the bound states which appear on the negative side of the real axis.

The computed resonance energies are collected in table 2 where the experimental values also are given. Three  $0^+$ -states appear, i.e. the ground state and two resonances. The first resonance is very close to the threshold with an extremely small width of about 62 eV. It is then difficult to distinguish from a discretized continuum state without information from its wavefunction. The second  $0^+$ -resonance appears around 4 MeV with a width of about 1 MeV. The real energy disagrees with previous experiments [3], but it is consistent with the analysis of the recent experiment [7, 1] as quoted in table 2.

We find four  $2^+$ -states, i.e. one excited bound state and three resonances. Only two resonances are suggested by experiments [3,7,1]. With the natural choice of  $b = 6$  fm the highest of the computed resonances can easily be adjusted to the experimental value [7,1]. It would perhaps be natural to adjust the lowest resonance to the measured energy. However, an attempt to do this failed because a smaller attraction than given in table 2 move the energy upwards but at the same time the top of the confining barrier is approached and exceeded leading to much faster increase of the width. The result is that the width increases quickly whereas the energy remains essentially unchanged. The same behavior is seen for the second of the  $2^+$ -resonances. Only the third follows naturally the experimental specifications with this choice of one three-body interaction of the present Gaussian form.

We find two  $4^+$ -resonances. If the three-body strength is reduced from the value in table 2 the widths of both resonances increase dramatically around 4 MeV and 9 MeV, respectively. Therefore the most consistent solution is that the highest  $4^+$ -resonance is found experimentally while the lowest has been hidden behind other states in previous experiments. Consequences of allowing variation of  $b$  are discussed in section 4.

Two  $1^+$  resonances are known experimentally, where the 7.84 MeV state is an isospin  $T = 1$  state. The two calculated  $1^+$ -resonances are artificial in the sense that only one of these resonances is found in the calculation, since a state with  $T = 1$  cannot be described by our formalism. The energy is then adjusted through the three-body potential to either of the measured values corresponding to isospin zero or one. The fact that only one state is found in the computation reflects that we only have the correct degrees of freedom to describe  $T = 0$  states. The reason for also adjusting to the  $T = 1$  energy is the expectation that the decay into three  $\alpha$ -particles would occur through the same intermediate and large-distance structures as for  $T = 0$ . We do not imply that the  $T = 1$  state has the same structure at small distances.

All other states than  $J^\pi = 0^+, 2^+, 4^+$  only appear once. Their energies are then adjusted by use of the three-body potential and the related width for the range of  $b = 6$  fm can be compared to the measured values. Since only one  $2^-$  and one  $4^-$ -resonance appear we suggest that the uncertain assignment of the second experimental  $2^-$ -resonance should be changed to  $4^-$ . The  $3^+$  and  $6^+$  states are not known experimentally and we can only make rough guesses of the three-body strength. Since  $6^+$  belongs to the family of even angular momenta and even parity we used a similar strength of  $-20$  MeV. The unnatural parity of  $3^+$  puts it in the same class as the  $1^+$  state but the strength of  $-20$  MeV already leads to an energy of about 6 MeV. This  $3^+$  estimate is then very uncertain.

It is remarkable that the ratio between theoretical and experimental values for the widths in almost all cases is around 2. The widths are in most cases fairly well estimated by the tunneling probabilities through the respective barriers shown in fig. 1, see [36]. This corresponds to an exponential dependence on energy and deviations

within a factor of two can then be considered to be very accurate [36]. These results are obtained without special treatment of the small distance properties beyond that corresponding to the  $3\alpha$ -structures. The possibility of preformation factors or  $\alpha$ -particle spectroscopic factors, as appearing in ordinary  $\alpha$ -decay, seems to play a minor role. It is interesting to note that we systematically calculate slightly too large widths indicating preformation factors at the surface of about  $1/2$ .

Two exceptions from the general rule are seen in the second  $0^+$  and the two  $1^+$  resonances, where the computed width is 3.4 times smaller for  $0^+$  and larger for the two  $1^+$  states by  $2.6 \cdot 10^3$  and  $5.3 \cdot 10^5$ , respectively. The  $1^+$  states require in contrast to all the other states preformation (spectroscopic) factors three and five orders of magnitude smaller than for the other states. This reflects totally different structures corresponding to a full break down of the  $3\alpha$ -descriptions at small distances. This is particularly pronounced for the  $T = 1$  state which cannot be described by the  $T = 0$   $\alpha$ -particle building blocks. The preformation factor correspondingly comes out as exceedingly small.

The different structure is less obvious for the lowest  $1^+$  state with  $T = 0$  which is not forbidden for symmetry reasons in the  $3\alpha$ -models. However, a strong hint is found in the model by the unusually large lowest possible hypermomentum of 8. The immediate guess of  $K = 1$  for  $1^+$  states are ruled out, together with all other hypermomenta below  $K = 8$ , by the imposed boson symmetry of the three  $\alpha$ -particles [37]. This is in clear contrast to all the other  $J^\pi$  states where the lowest hypermomentum consistent with angular momentum always contribute, see table 1.

These results are also, apart from the  $1^+$  anomalies, remarkable for at least one other reason, i.e. a monotonic dependence on energy, angular momentum and parity does not exist. The barriers in hyperradius provided by the calculation must then be physically reasonable, in turn implying that the concept of the hyperspheric adiabatic expansion is in rather close agreement with the physical process. The systematic correlation with the experimental widths, varying by orders of magnitude, is otherwise totally unexplained. It should here be emphasized that many of the resonances are not well described as cluster states [11]. This is particularly clear for the two  $1^+$  states.

The three-body potentials with  $b = 6$  fm seem to fall in two groups, i.e. one with a strength  $S$  of about  $-20$  MeV ( $0^+$ ,  $2^+$ ,  $3^+$ ,  $4^+$ ,  $6^+$ ) and one with  $S \approx -2$  MeV ( $1^-$ ,  $2^-$ ,  $3^-$ ,  $4^-$ ). This should indicate that the amount of  $\alpha$ -cluster states within each group is roughly the same as also reflected by the comparison of calculated and known widths. Exceptions are the  $1^+$  states with much larger strengths of about  $-80$  MeV. The computed widths for these states increase substantially with the range  $b$  of the three-body parameter when the strengths correspondingly are increased to maintain the energy. The apparent spectroscopic factor for the isospin zero state would for  $b \approx 4$  fm be comparable to the values for the other states as reported in [36].

Beside the energy the size is a characteristic quantity for any system. This is straightforward for bound states but resonances decay and are therefore infinitely large. However, the complex scaling provides a simple measure of the extension of the small distance part of the wavefunction, i.e. expectation values related to the hyperradius. The usual relation is [22]

$$r_{rms}^2 = \frac{1}{12} \langle \Psi | \rho^2 | \Psi \rangle \exp(i2\theta) + R_\alpha^2, \quad (3)$$

where  $R_\alpha = 1.47$  fm and  $r_{rms}$  are the root mean square radii of the  $\alpha$ -particle and  $^{12}\text{C}$  in the  $3\alpha$ -model, respectively. The finite size of the three  $\alpha$ -particles are then accounted for. Complex rotation by  $\theta$  means that the square of the hyperradius is multiplied by  $\exp(i2\theta)$ . The expectation value in eq.(3) is then expressed in the rotated system, and now this quantity is finite. They are still complex numbers and the absolute square can be used as the measure of size. Another tempting possibility is to interpret the real part as the radius of the resonance and the imaginary part as the variation (uncertainty) of the radius of the continuum wavefunctions as energy changes through the interval  $E_R \pm \Gamma/2$  around the central energy [38].

The numerical results for the resonances and bound states are given in table 3 for both prescriptions. The real parts are in all cases very close to each other and certainly within the ‘‘uncertainty’’ measured by the imaginary part. For the two bound states the imaginary part reflects the small uncertainty in the numerical computation, since here the values should strictly be real. The ground state result is within the uncertainty identical to the root mean square radius of  $^{12}\text{C}$ , i.e. 2.468 fm. The ‘‘uncertainties’’ are small for narrow resonances and relatively large for broad resonances. The bound  $2^+$ -state is smaller than the ground state and all the resonances are larger. The  $0^+$  and  $2^+$ -resonances are especially large because they are built of the same partial waves and orthogonality then apparently push them outwards. The comparison to the old results derived from the resonating group method [39] and the ones from the generator coordinate calculation [16], as well as the recent computation [40] and the antisymmetrized molecular dynamics results from [11] are in agreement within the uncertainties. It should be emphasized that a detailed comparison should take the energy differences into account. From halo physics of neutral particles we know that energy and radius are closely correlated. The radial variation with binding energy is much smaller for charged particles and finite angular momentum.

### 3.4 Resonance structures

The resonance structure is determined by combining the amplitude obtained as the solution to the radial wavefunction with the individual structure of each adiabatic component. The real parts of the radial wavefunctions are shown in figs. 3 and 4 for the two bound states and each of the 14 resonances. At least two general features are

**Table 3.** Sizes expressed as root mean square radii (in fm) of the  $^{12}\text{C}$  bound states and resonances. The second column is  $\rho_{rms} = |\langle \rho^2 \rangle|^{1/2}$ , and the fourth column is without absolute squares of the expectation values. The third and fifth columns are root mean square radii of  $^{12}\text{C}$  states obtained by eq. (3) with the two different  $\langle \rho^2 \rangle$  prescriptions, respectively. The last four columns are computations from [11,39,16,40]. The root mean square charge radius of  $^{12}\text{C}$  ground state is  $\langle r^2 \rangle^{1/2} = 2.4829 \pm 0.0019$  fm [41].

$J^\pi$	$\rho_{rms}$	$r_{rms}$	$\langle \rho^2 \rangle^{1/2}$	$r_{rms}$	$r_{kan}$ [11]	$r_{kam}$ [39]	$r_{ueg}$ [16]	$r_{fun}$ [40]
$0_0^+$	7.39	2.59	7.35-i0.74	2.59-i0.00	2.53	2.468	2.40	2.40
$0_1^+$	12.19	3.81	12.14+i1.16	3.82-i0.02	3.27	3.56	3.40	3.83
$0_2^+$	11.35	3.59	10.80+i3.50	3.30+i1.20	3.98		3.52	
$1^+$	8.41	2.84	8.40-i0.43	2.84+i0.10	2.47			
$3^+$	8.95	2.97	8.79+i1.70	2.86+i0.64				
$2_0^+$	6.79	2.45	6.69-i1.14	2.45+i0.00	2.66	2.51	2.36	2.38
$2_1^+$	11.37	3.60	11.37+i0.11	3.54+i0.53	3.99		3.52	
$2_2^+$	11.90	3.74	11.73+i2.00	3.53+i1.05	3.50	4.1	3.34	
$2_3^+$	11.90	3.74	11.73+i2.00	3.53+i1.05	3.86			
$4_1^+$	10.19	3.29	10.19+i0.11	3.27+i0.29	2.71	2.31	2.29	2.31
$4_2^+$	8.68	2.91	8.68-i0.01	2.89+i0.21	4.16	2.44	3.64	
$6^+$	9.49	3.11	9.44+i1.04	3.01+i0.62				
$1^-$	10.24	3.30	10.22+i0.66	3.26+i0.43	3.42	3.45	3.29	
$2^-$	10.11	3.27	10.02+i1.39	3.18+i0.61	3.49		3.32	
$3^-$	9.33	3.07	9.33+i0.10	3.06+i0.20	3.13	2.87	2.83	
$4^-$	9.03	2.99	9.02+i0.51	2.93+i0.47	3.19		2.87	

striking. First, only very few of these wavefunctions contribute significantly. Furthermore, for all states one adiabatic component is much larger than all other contributions. This reflects the rather fast convergence of the adiabatic expansion where three eigenvalues often provide an accurate solution. Second, the wavefunctions oscillate with exponentially decreasing amplitudes as functions of  $\rho$ . This behavior is qualitatively the same for bound states and resonances which precisely is the reason for using complex scaling to compute resonance wavefunctions and energies. The imaginary parts are not shown to avoid cluttering the figures. They exhibit similar oscillatory behavior.

The probabilities for finding the different adiabatic components in each resonance wavefunction are given in table 4. The structures of the resonances are then essentially contained in these dominating angular wavefunctions, where each is related to one adiabatic potential. For each resonance we therefore take the dominating contribution and decompose into the partial waves specified in table 1. These partial wave decompositions are shown in figs. 5 and 6. The overall feature is that the dependence on hyperradius is rather strong. However, we should emphasize that the small distance structure only has little physical significance. Numerically the variation arises from couplings of low-lying adiabatic potentials which change rapidly in this region due to the different behavior of  $s$ ,  $d$  and  $g$  two-body potentials imposed by the different behavior of the phase shifts.

The two dominating wavefunctions for the  $0^+$ -resonances have very different behavior. The first is dominated by  $\ell_x = \ell_y = 0$  at about 10 fm, but at larger  $\rho$  the higher partial waves all become almost equally important. The large-distance behavior is consistent with the description of one  $\alpha$ -particle far away from a spatially confined  $^8\text{Be}(0^+)$ -

**Table 4.** Contribution  $W_n$  of each adiabatic potential, labeled by  $n$ , to the total norm of the wave function of each  $^{12}\text{C}$ -state. Only those contributions of more than 1% are given.

$J^\pi$	$W_1$	$W_2$	$W_3$
$0_0^+$	2	98	
$0_1^+$	15	84	
$0_2^+$	96	4	
$1^+$	100		
$2_0^+$		100	
$2_1^+$	100		
$2_2^+$		94	7
$2_3^+$	1		99
$3^+$	99	1	
$4_1^+$	97	3	
$4_2^+$		97	3
$6^+$			
$1^-$	88	12	
$2^-$	99		
$3^-$	99	1	
$4^-$	100		

structure. The higher partial waves arise from  $s$ -waves in the “unnatural” Jacobi systems. The second wavefunction has about equal contributions at small  $\rho$  from  $\ell_x = \ell_y = 0, 2$ , but at large  $\rho$  the  $s$ -wave component increases strongly while the higher partial waves correspondingly decrease towards zero. This large-distance structure is consistent with all three  $\alpha$ -particles symmetrically distributed far from each other.

The first of the other natural parity wavefunctions, corresponding to  $1^-$ ,  $3^-$ ,  $2^+$ ,  $4^+$  and  $6^+$ , all have  $\ell_x = 0$  as the dominating component at large distance. This is

consistent with a  $^8\text{Be}(0^+)$ -structure and the third particle with  $\ell_y$  equal to the total angular momentum. Several other components are small and of comparable magnitude. The lowest  $0^+$ -wavefunction also falls into this category.

The first wavefunctions for unnatural parity,  $1^+$ ,  $3^+$ ,  $2^-$ ,  $4^-$ , all have  $\ell_x = 2$  as the dominating component both at small and large distances. The angular momentum,  $\ell_y$ , of the third particle for this component is as small as possible consistent with the total spin and parity. Only one more component gives significant contributions for each of these states, i.e.  $\ell_x = 4$  combined with the lowest possible  $\ell_y$  for  $1^+$  and  $4^-$ , and  $\ell_x = 2$  and  $\ell_y = 3$  for  $2^-$ . The latter component is larger than the contribution from the higher partial wave of  $\ell_x = 4$  and the lowest possible  $\ell_y$ -value of 3.

The third  $2^+$ -wavefunction is similar in structure with one dominating component of  $\ell_x = 2$  and  $\ell_y = 0$ , and another component of half the size with  $\ell_x = 2$  and  $\ell_y = 4$ . Here the component with  $\ell_x = 2$  and  $\ell_y = 2$  only contributes insignificantly. The second  $2^+$ -wavefunction has three about equal contributions at large distance from  $(\ell_x, \ell_y) = (0, 2), (2, 0), (2, 2)$ . The second  $4^+$ -wavefunction also has three comparable contributions from  $(\ell_x, \ell_y) = (0, 4), (4, 0), (2, 2)$ , and in addition several smaller components.

We emphasize that the contributions from the individual adiabatic potentials should be combined with their respective amplitudes to give the total structure of the resonances. These amplitudes depend on hyperradius and the probabilities in table 4 are averages over all  $\rho$ . The exponential decrease with  $\rho$  then obviously heavily enhances the structures at the small distances. The relative distributions at larger distances may change substantially.

The different partial waves receive contributions from different adiabatic components. The probabilities given in table 2 can be obtained by combining the information in figs. 5 and 6, and figs. 3 and 4. The results reflect the conclusions from the above discussion.

## 4 Interaction dependence

We have to distinguish between two types of inaccuracies, i.e. arising from (i) inaccuracies in the numerical computations for given sets of input parameters, and (ii) model assumptions and uncertainties in the corresponding parameters. Here the uncertainties in (i) originate from cut-offs in different basis expansions, i.e. the partial waves and the number of Jacobi polynomials for each of the three Faddeev components, and the number of adiabatic potentials. The convergence can be seen directly in the decreasing amplitudes for both partial waves and adiabatic potentials. We emphasize that the contributing terms vary with hyperradius as discussed in the previous section. Also the rotation angle should be chosen as small as possible to optimize accuracy while still allowing distinction of the three-body resonance from the background continuum states.

Model uncertainties are more difficult to assess. We shall first consider those intrinsic to the cluster model,

and afterwards compare to experiments and other more microscopic computations.

### 4.1 The $3\alpha$ -cluster model

The model uncertainties are essentially related to the different choices of interactions reproducing the low-energy  $\alpha - \alpha$  scattering properties. The Ali-Bodmer potentials with the correct number of two-body bound states are constructed with repulsive cores to simulate the effect of Pauli forbidden states. The radial dependence then varies from being strongly repulsive to fairly attractive implying rapidly varying adiabatic potentials with (avoided) crossings. To test the sensitivity we constructed a purely attractive potential “attr” with the two-body complex resonances energies,  $(E_R, \Gamma) = (100, 0.01)$  keV,  $(3.2, 1.4)$  MeV, and  $(11.6, 3.9)$  MeV in  $\ell = 0, 2, 4$  waves, respectively. These values are rather close to the measured values. We furthermore constructed the potential “AB(a’d’)” by combining the two-body  $s$  and  $d$ -waves from another Ali-Bodmer potential while substituting the  $g$ -wave by the above attractive potential. This potential has  $\ell = 0, 2, 4$   $^8\text{Be}$ -resonances at  $(E_R, \Gamma) = (90, 0.006)$  keV,  $(3.0, 1.4)$  MeV, and  $(11.6, 3.9)$  MeV, respectively.

The angular eigenvalues for different potentials are compared in fig. 7 for some of the resonances. The striking feature is that the large-distance behavior of the spectra is the same. First the eigenvalues increase linearly with hyperradius simply because the leading order is the Coulomb potential multiplied by  $\rho^2$ . Second the coinciding spectra at large distances reflect that the resonance positions are crucial. These in turn essentially only depend on the two-body scattering lengths. Both spectra and resonance energies are to leading order then roughly model independent as determined by the low-energy two-body scattering properties.

The complex resonance energies are compared in fig. 8 for different interactions. First for the  $0^+$ -resonances we modestly only change (from AB(a’) to AB(a’d’)) the  $s$ -waves a little while both  $d$  and  $g$ -potentials are quite different. The result is that the energies essentially are unchanged for these potentials. The recently found experimental result has an unusually large width of about 3.4 MeV [7,1]. This is somewhat larger but still comparable with the widths found from inelastic  $\alpha - \alpha$  scattering experiments [5,6]. We then investigate the dependence on the three-body interaction. We follow the resonance as function of the three-body strength for fixed values of the range. As the energy increases also the width increases almost along the continuum background spectrum. If we instead keep the energy of the lowest  $0^+$ -resonance by correlated changes of three-body strength and range, the second  $0^+$ -resonance moves relatively little in position while the width increases strongly. If both the measured position and the unusually large width should be reproduced the range has to be very large and the necessary rotation angle would not be numerically accessible.

For the  $2^-$ -case we compare results from the same two interactions where we find one resonance at roughly the

same position and width in both case. This is more striking now where the dominating components have  $\ell_x = 2$  in contrast to  $0^+$  where the similar  $\ell_x = 0$ -components dominate. The variation with three-body strength is rather similar. The resonance position can easily be adjusted with reasonable parameters in a fairly large interval around 5 MeV. Thus even quite different potentials with the same two-body resonances give roughly the same three-body structure.

For the  $2^+$ -resonances we compare in fig. 8 the results for AB(a') with the results from, attr, a very different potential with only attraction in all partial waves. First we note that the resonance positions vary differently with the three-body interaction when we use the initial Ali-Bodmer potential. The lowest only moves a little and essentially parallel to the background continuum. The second resonance has a strong tendency to move into the continuum reflecting the quickly increasing width as a consequence of a decreasing barrier. The third resonance moves faster but in the region of the measured energy and width.

Second it is remarkable that the very different purely attractive potential also leads to one bound state and three resonances in the same energy region. Again the lowest resonance is very close to the  $3\alpha$ -threshold, and even below for a fairly weak attractive three-body potential. In this case it would seem natural to use a repulsive three-body interaction but then the bound state is too easily pushed up into the continuum. The level spacing is too small as for most other cluster models. The variation with three-body potential is similar to the behavior seen for the other potential. Now the second and third resonance positions are somewhat closer. From these energy variations it is then again natural to associate the highest-lying to the experimentally found resonance [7, 1], and fix its position by adjusting the three-body strength for different values of the range. The width of this resonance and both positions and widths of the other two resonances are then determined.

For the  $4^+$ -resonances and the initial Ali-Bodmer potential we notice the same behavior as for the  $2^+$ -resonances, i.e. the lowest tends to increase the width quickly and disappear into the background whereas the highest moves faster with the three-body strength in the region of the measured energy and width. This is again due to the structure of the potential. The resonance energy in the minimum is pushed up towards the top of the barrier where the width increases dramatically. The highest  $4^+$ -resonance can then, in contrast to the lowest, rather easily be moved to the experimental position by adjusting the three-body strength.

For the purely attractive potential we have to choose a repulsive three-body interaction if no three-body bound states should appear. With the same range of  $b = 6$  fm the dominating potential has a high and thick barrier leading to a very small width. Instead of an arbitrary adjustment of the range for this particular case we use the same ranges and a similar attractive three-body potential. The  $4^+$  bound state in fig. 8 should then be considered spurious and discarded. Then again two resonances appear

with energies below 8 MeV and widths varying from almost zero to almost 2 MeV. This is within a factor of two from the results of the initial Ali-Bodmer potential.

The structures of the resonances are reflected in their partial wave decompositions. The large-distance properties of the eigenvalues are almost identical for interactions with the same two-body resonances, and consequently the partial wave components also coincide for large hyperradii. However, it is also obvious that when the short-distance properties are qualitatively different then the adiabatic potentials must reflect those differences.

We compare the quantitative differences in fig. 9 for some of the adiabatic potentials. For  $0^+$ -states the  $s$  and  $d$ -waves dominate and the change into an attractive  $g$ -wave has only a small effect except at very small hyperradii. For the  $2^+$ -states we compare results where all partial wave two-body interactions are different. Nevertheless, the partial wave decompositions for the three lowest adiabatic potentials are remarkably unaffected. The same behavior of invariant large-distance properties and relatively little variation at small distance is found for the  $4^+$  and  $2^-$ -states.

The other resonances are all easily moved to the desired position by the three-body interaction, and the widths are strongly correlated with the measured values, as in table 2. The structures of these resonances are also very insensitive to the specifics of the interactions. The  $6^+$ -resonance seems consistently to fall at an energy of about 6 MeV which is in the upper end of the considered energy interval. This estimate has about the same uncertainty as the other natural parity even angular momenta states. They are all built on the same low angular momentum partial waves, see table 1. The additional uncertainty is due to the less known two-body interactions of higher angular momentum. The  $3^+$ -resonance is much more uncertain since the necessary three-body potential could vary from almost vanishing to values similar to that of  $1^+$ .

We can now summarize how resonance energies and structures are influenced by two-body interactions reproducing the low-energy scattering properties. First the number of resonances remain unchanged within approximately the same region of complex energies. Their energies may vary by modest amounts. One exception is the  $4^+$ -states with the purely attractive potential where the bound state has to be discarded as Pauli forbidden. The structures of the adiabatic potentials are rather insensitive to the specific interaction except at small hyperradii corresponding to distances where the three  $\alpha$ -particles overlap substantially. The relative contributions of the adiabatic potentials may vary at small distances where the contributions to the resonances are rather small.

In particular, the insensitive properties are that (i) the bound and the lowest  $0^+$ -states are related to the same adiabatic potential differing by one radial oscillation, (ii) the bound and the second  $2^+$ -states also are related to the same adiabatic potential differing by one radial oscillation, (iii) the second  $0^+$ -resonance and the first (bound)  $2^+$  state have no radial nodes and both are related to adiabatic potentials different from those associated to the

lowest resonances, (iv) the third  $2^+$ -state has no radial nodes and it is related to a third adiabatic potential, (v) all states only appearing once are related to the lowest adiabatic potential without radial nodes.

## 4.2 Other models

All angular momenta and parities are also considered in some previous model computations. The basic problem in comparison is that the interactions often are different in the many investigations. However, the parameters are always chosen to reproduce some measured quantities. The shortcoming of such an approach is in general that misinterpreted data inadvertently can be used both to fit the interactions and afterwards to compare to model results. To illustrate the variation of the model predictions we discuss some results from selected representative methods which all to some degree include the underlying microscopic nuclear structure.

The formulation from antisymmetrized molecular dynamics [11] seems first to aim at reproducing the bound state properties. The low-energy excited spectrum then differs from ours only by one less  $2^+$ -resonance. The level spacing is a little larger, and the  $1^+$  and the last  $4^+$ -states are found close to 17.5 MeV. We find all our states below 16 MeV and the spacing between the two bound states too small. Our philosophy is that the ground state has contributions beyond the  $3\alpha$ -cluster structure and we should not necessarily reproduce its energy. In the newest preprint [11] the spectrum has changed reflecting the use of different interactions. Now the number of resonances with given angular momentum and parity below 16 MeV are the same as in the present model.

The method of fermionic molecular dynamics is less developed in practical applications [12]. They find one less  $2^+$ ,  $1^+$  and  $4^-$ -resonance than us below 15 MeV.

An older publication using the generator coordinate method found many resonances below 15 MeV [15,16]. They found one less  $2^+$  than us, and otherwise the same number of states in this spectrum. The generator coordinate method has recently been used extensively to investigate the structure of light nuclei [13]. The focus is here on the bound states and the lowest resonances. The two bound states are too close-lying, and the number of resonances are too few both compared to experiments and to our results. Below 15 MeV they find only one  $0^+$ , no  $1^+$ , one  $2^+$ , and no  $2^-$ . Furthermore, their sequence has very little resemblance with the measured spectrum.

The algebraic cluster model is based on group theory [14]. Two more states have appeared in the last publication close to an excitation energy of 15 MeV. Below 15 MeV they find the same spectrum as us except for one less  $4^+$ -state. The overall spacing is therefore almost the same. The spectrum is computed from a model with 3  $\alpha$ -particles in an equilateral triangle where rotation-vibration interactions, Coriolis forces and vibration-vibration interactions are needed.

## 4.3 Experiments

In confronting the results in table 2 with experimental input the predicted low-lying  $2^+$ -states and the lowest  $4^+$ -state stand out as problematic. However, experimentally there is not presently a consensus on the position of  $2^+$ -resonances in  $^{12}\text{C}$ ; as previously mentioned different probes find states at different energies. To some degree this might simply reflect selection rules or structural effects in different experiments, but when the same probe sees different states in different experiments (as for  $^{12}\text{C}(\alpha,\alpha)^{12}\text{C}$  [5, 6]), there is clearly a problem. It seems safe to infer from the data that a broad  $2^+$ -state exists in the region 14-15 MeV as e.g. seen in  $\beta$ -decay [7,1] and in some scattering experiments[3], but whether more broad states exist near 10 MeV overlapping with the known broad  $0^+$ -state, as suggested by [6], is unclear. If so they must be feebly fed in the  $\beta$ -decays as suggested in [11]. The large width of the second  $0^+$ -resonance is qualitatively in agreement with the results of about 2.7 MeV obtained from the inelastic scattering experiments [5,6]. The existence of narrow states below 10 MeV can be ruled out experimentally. The existence of a broad  $4^+$ -state below the known one at 14.1 MeV cannot be ruled out experimentally; for comparison the broad  $0^+$ -state centered at 10 MeV is not seen in a number of transfer reactions due to its large width – it is most clearly seen in  $\beta$ -decay experiments where a  $4^+$ -state cannot be favorably populated.

## 5 Summary and conclusions

We employ the established method of hyperspherical adiabatic expansion in combination with complex scaling to compute the energies and widths of  $^{12}\text{C}$ -resonances below 15.96 MeV. We use the  $3\alpha$ -cluster model with well known angular momentum dependent two-body interactions adjusted to reproduce the low-energy  $\alpha - \alpha$  scattering properties. Obviously then only three-body properties can be computed, but within this overall constraint, the model can be applicable even when many-body properties are important. The partial waves of each contributing Faddeev component are expanded on a large complete basis of Jacobi polynomials. Only very few adiabatic potentials are needed for convergence for each angular momentum and parity  $J^\pi$ .

The energies are determined by the behavior of the potentials at small distances. At intermediate distances the potential has a barrier that determines the resonance width. As mentioned, the two-body potential is chosen to reproduce the low-energy two-body scattering properties, and a three-body short-range interaction is also added. This accounts for the intrinsic nucleonic degrees of freedom by producing a correct boundary condition at small distances matching the  $3\alpha$ -structure at large distance. However, it does not describe the short-distance structure properly and hence electromagnetic transitions can not be expected reliably estimated in this model.

In our three-body cluster model we add three-body potentials to place the resonances at the desired positions.

These potentials are chosen independently for each  $J^\pi$  to depend only on the hyperradius. We use one Gaussian with a range  $b = 6$  fm corresponding to the distance when three  $\alpha$ -particles touch each other in an equilateral triangle. The strength is used to place one of the resonances at the desired energy. This invention opens the cluster model for applications to many-body resonances similar to the simple  $\alpha$ -emission model.

We are not concerned with the bound states where especially the ground state can deviate more from a  $3\alpha$  cluster state than most of the excited states and here in particular from the first  $0^+$  resonance. We focus instead on reproducing the correct energy and investigate the systematics of the strongly correlated corresponding width. Designing a three-body potential to fit simultaneously more of the states would not provide any more insight. The resonance structures are essentially independent of these three-body potentials.

The model leads to a number of low-lying resonances for each  $J^\pi$ , i.e. two  $0^+$ , three  $2^+$ , two  $4^+$ , and one of each of  $1^\pm$ ,  $2^-$ ,  $3^\pm$ ,  $4^-$ , and  $6^+$ . Dependence on the two and three-body interactions are investigated. The conclusions are that the highest of the  $2^+$  and  $4^+$  resonances most naturally can be placed at the measured values whereas the lowest of these resonances acquire a very large width when they are pushed towards higher energies. In fact the confining barriers of the adiabatic potentials vanish before the energy is high enough.

The structures of the individual resonances are almost totally independent of the three-body potential or equivalently independent of the resonance positions. On the other hand, the energies and widths are strongly correlated and rather insensitive to the structure. With the AB(a') Ali-Bodmer potential and the measured energies reproduced with a three-body potential of range for  $b = 6$  fm, the widths are all systematically about a factor of two larger than measured indicating a corresponding spectroscopic factor of about 0.5. Two exceptions appear, i.e. the second  $0^+$  resonance with a computed width about 3 times smaller than a recent measurement, and the two  $1^+$  resonances with 3 – 5 orders of magnitude larger computed widths and the corresponding very small spectroscopic factors.

One of each of the negative parity states is found suggesting that the tentative assignment of one of the  $2^-$ -resonances should be changed to  $4^-$ . The large computed width of the second  $0^+$ -resonance appears in the same energy region as several other resonances. The two lowest  $2^+$  and the lowest  $4^+$  resonances are presumably impossible to reconcile with the experimental information. The energies of both the lowest  $2^+$  and  $4^+$ -resonances should presumably be higher. This can be achieved by using a three-body interaction depending on more than the hyperradius. However, in the present work the focus is on the structure and the relation between energies and widths.

The simple three-body cluster model is, perhaps surprisingly, doing as well as more microscopic models. The difference is really that the phenomenology is inserted on the nucleonic level for microscopic models. These micro-

scopic models are more likely to have problems with spatially extended systems, and elaborate calculations of observables. Our cluster model exploits the experimental information by inserting the phenomenology on the  $\alpha$  cluster level and a few of the  $^{12}\text{C}$  properties are used as well. This model is still technically difficult but closer to the observables since we adjust on the three-body level without structure changes.

The discrepancies between experimental and theoretical results can logically be related to either experiments or theory or to a combination of both. Cleaning up on the experimental side to achieve consistency between different experiments is necessary. This is especially in connection with the possibly overlapping resonances around 4 MeV. The present model does not treat the intrinsic degrees of freedom. They are accounted for on the two-body level by phenomenologically adjusted interactions, and on the three-body level by the hyperradial and  $J^\pi$  dependent potential. The most likely suspect is the simplicity of the three-body interaction which is supposed to mock up the important effects of the nucleonic degrees of freedom. The Pauli exclusion, when three  $\alpha$ -particles are close, is perhaps not well described. The one-Gaussian structure may be too simple, and the potential should perhaps depend on angular momentum quantum numbers or on individual adiabatic potentials.

In conclusion, we find in the present model a comparable number of resonances as in more microscopic calculations but the detailed energy spectra vary substantially between the different models. We find more low-lying resonances than measured. The partial wave structures of our resonances are very robust independent of their energies. We have established resonance structures and suggested the most likely energies within the model.

The real test is then to compare experiment and theory for observables with strong structure dependence. This would demonstrate which of the computed resonances are really seen in experiments. The obvious, and perhaps the only, observable for this is the momentum distributions of the  $\alpha$ -particles after decay of the resonances. Experimentally this has to be both accurate and kinematically complete. Theoretically large-distance continuum properties must be accurately computed and the present technique is at the moment the closest to provide answers. Both the necessary experiments and calculations are challenging but possible and both within reach.

## Acknowledgments

One of us ( R.A.R.) acknowledges support by a post-doctoral fellowship from Ministerio de Educación y Ciencia (Spain).

## References

1. C. Aa. Diget, PhD-thesis, Natural Science Faculty, University of Aarhus, 2006, and to be published.
2. H.O.U. Fynbo et al., *Nature* **433** (2005) 136.
3. F. Ajzenberg-Selove, *Nucl. Phys.A* **506** (1990) 1, and [http://www.tunl.duke.edu/nucldata/chain/12\\_newv.shtml](http://www.tunl.duke.edu/nucldata/chain/12_newv.shtml)

4. C. Kurokawa and K. Kata, Nucl. Phys. **A 738** (2004) 455; J. Phys.**G 31** (2005) s1907.
5. B. John, Y. Tokimoto, Y.-W. Lui, H. L. Clark, X. Chen, and D. H. Youngblood, Phys. Rev. **C 68**, 014305 (2003).
6. M. Itoh et al., Nucl. Phys.**A 738** (2004) 268.
7. C. Aa. Diget et al., Nucl. Phys.**A 760** (2005) 3.
8. P. Navratil, J.P. Vary, and B.R. Barrett, Phys. Rev. **C 62** (2000) 054311.
9. H. Matsumura and Y. Suzuki, Nucl. Phys.**A 739** (2004) 238.
10. S.C. Pieper, Nucl. Phys.**A 751** (2005) 516.
11. Y. Kanada-En'yo, Phys. Rev. Lett. **81** (1998) 5291. preprint arXiv:nucl-th/0605047
12. T. Neff and H. Feldmeier, Nucl. Phys.**A 738** (2004) 357.
13. P. Descouvemont, Nucl. Phys.**A 709** (2002) 275.
14. P. Bijker and F. Iachello, Phys. Rev. **C 61** (1999) 067305 and Annals of Physics **298** (2002) 334.
15. E. Uegaki, S. Okabe, Y. Abe, and H. Tanaka, Prog. Theor. Phys. **57** (1977) 1262.
16. E. Uegaki, S. Okabe, Y. Abe, and H. Tanaka, Prog. Theor. Phys. **62** (1979) 1621.
17. D. V. Fedorov and A. S. Jensen, Phys. Lett. **B389** (1996) 631.
18. D.V. Fedorov, A.S. Jensen and H. Fynbo, AIP conference proceedings **644**, 20-23 (2002).
19. D.V. Fedorov, H.O.U. Fynbo, E.Garrido and A.S. Jensen, Few-body systems, **34**, 33-37 (2004).
20. E. Garrido, D.V. Fedorov and A.S. Jensen, Phys. Rev. Lett. **96**, 112501 (2006).
21. E. Garrido, D.V. Fedorov, A.S. Jensen and H.O.U. Fynbo International Few-Body Conference, Brazil 2006, Nucl. Phys. **A**.
22. E. Nielsen, D.V. Fedorov, A.S. Jensen and E. Garrido, Phys. Rep. **347** (2001) 373.
23. A.S. Jensen, D.V. Fedorov, H.O.U. Fynbo and E. Garrido, AIP Conference Proceedings **791**, 164-173 (2005).
24. E. Garrido, D.V. Fedorov and A.S. Jensen, Nucl. Phys. **A 708**, 277-299 (2002).
25. E. Garrido, D.V. Fedorov and A.S. Jensen, Nucl. Phys. **A 700**, 117-141 (2002).
26. E. Garrido, D.V. Fedorov and A.S. Jensen, Nucl. Phys. **A 733**, 85-109 (2004).
27. E. Garrido, D.V. Fedorov, H.O.U. Fynbo and A.S. Jensen Nucl. Phys. **A**, in press.
28. E. Garrido, D.V. Fedorov, A.S. Jensen and H.O.U. Fynbo, Nucl.Phys. **A 748**, 27-38 (2005).
29. E. Garrido, D.V. Fedorov, A.S. Jensen and H.O.U. Fynbo, Nucl.Phys. **A 748**, 39-58 (2005).
30. E. Garrido, D.V. Fedorov, A.S. Jensen and H.O.U. Fynbo, Nucl.Phys.**A 766**, (2005) 74-96.
31. S. Ali and A.R. Bodmer, Nucl. Phys. **80** (1966) 99.
32. H. Arenhövel, J. Carbonell, L. Canton, A. Fonseca, W. Glöckle, H. Hofmann, A. Kievsky, W. Leidemann, G. Orlandini, R. Timmermans, and M. Viviani, preprint arXiv:nucl-th/0412039.
33. S.I. Fedotov, O.I. Kartavtsev and A.V. Malykh, Eur. Phys. J. **A 26** (2005) 201.
34. S.I. Fedotov, O.I. Kartavtsev, V.I. Kochkin and A.V. Malykh, Phys. Rev. **C 70** (2004) 014006.
35. D.V. Fedorov, A. Cobis and A.S. Jensen, Phys. Rev. **C 59** (1999) 554.
36. D.V. Fedorov, A.S. Jensen and H. Fynbo, Nucl. Phys.**A 713** (2003) 685c.
37. A.A. Korshennikov, Sov. J. Nucl. Phys. Nucl. Phys. **52** (1990) 827.
38. N. Moiseyev, Phys. Rep. **302** (1998) 212.
39. M. Kamimura, Nucl.Phys.**A 351** (1981) 456.
40. Y. Funaka, H. Horiuchi, P. Schuck, G. Röpke, Eur. Phys. J. **A 24** (2005) 321.
41. W. Ruckstuhla et al., Nucl.Phys.**A 430** (1984) 685-712.

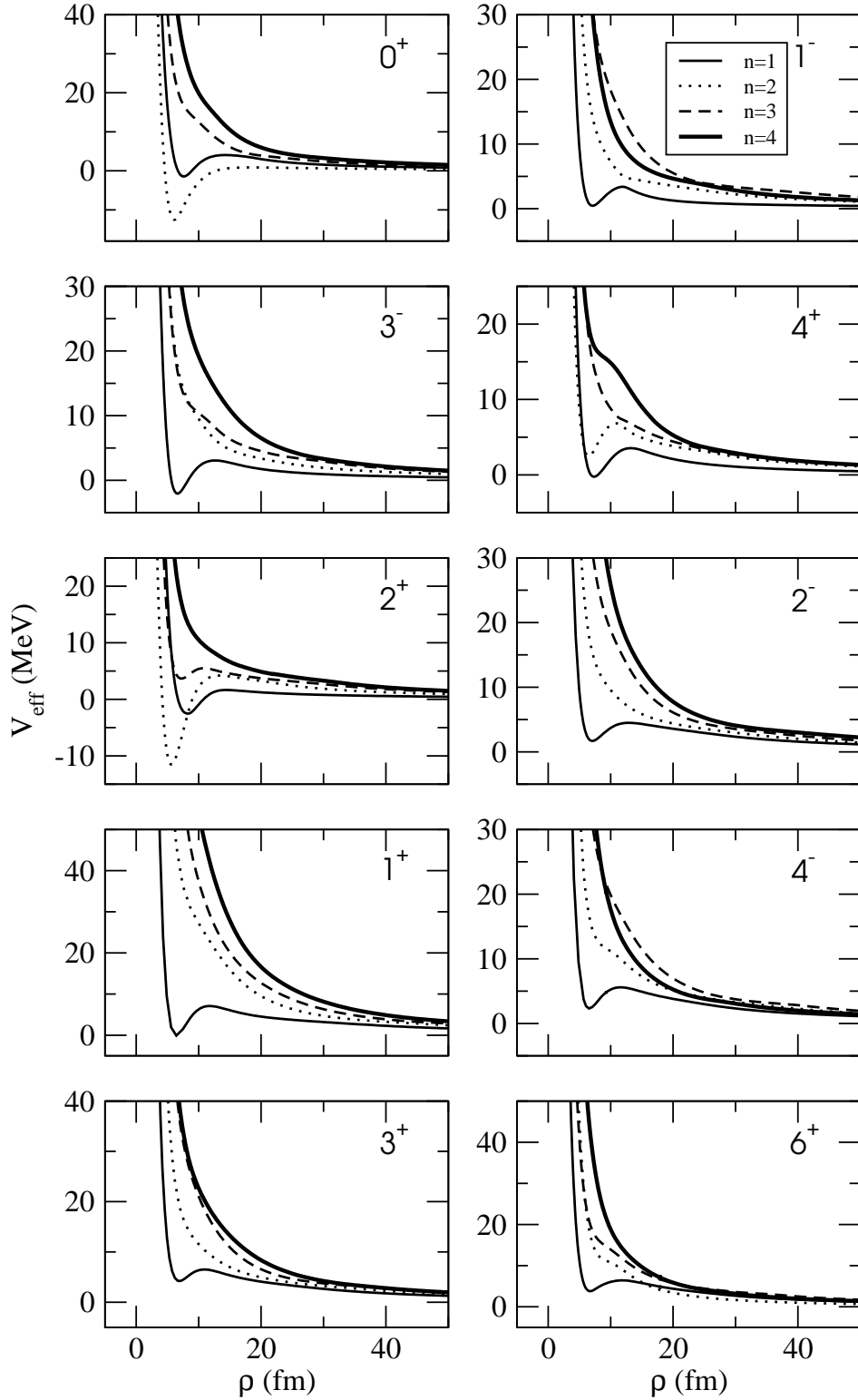


**Fig. 1.** The real parts of the four lowest adiabatic effective potentials, including the three-body potentials, as functions of  $\rho$  for the  $^{12}\text{C}$  resonances with  $J^\pi$  given in the figures. The two-body interaction, obtained from [17], is a slightly modified version of the  $a_1$ -potential of [31]. The parameters ( $S$  and  $b$ ) of the three-body Gaussian potentials,  $S \exp(-\rho^2/b^2)$ , are given in table 2.

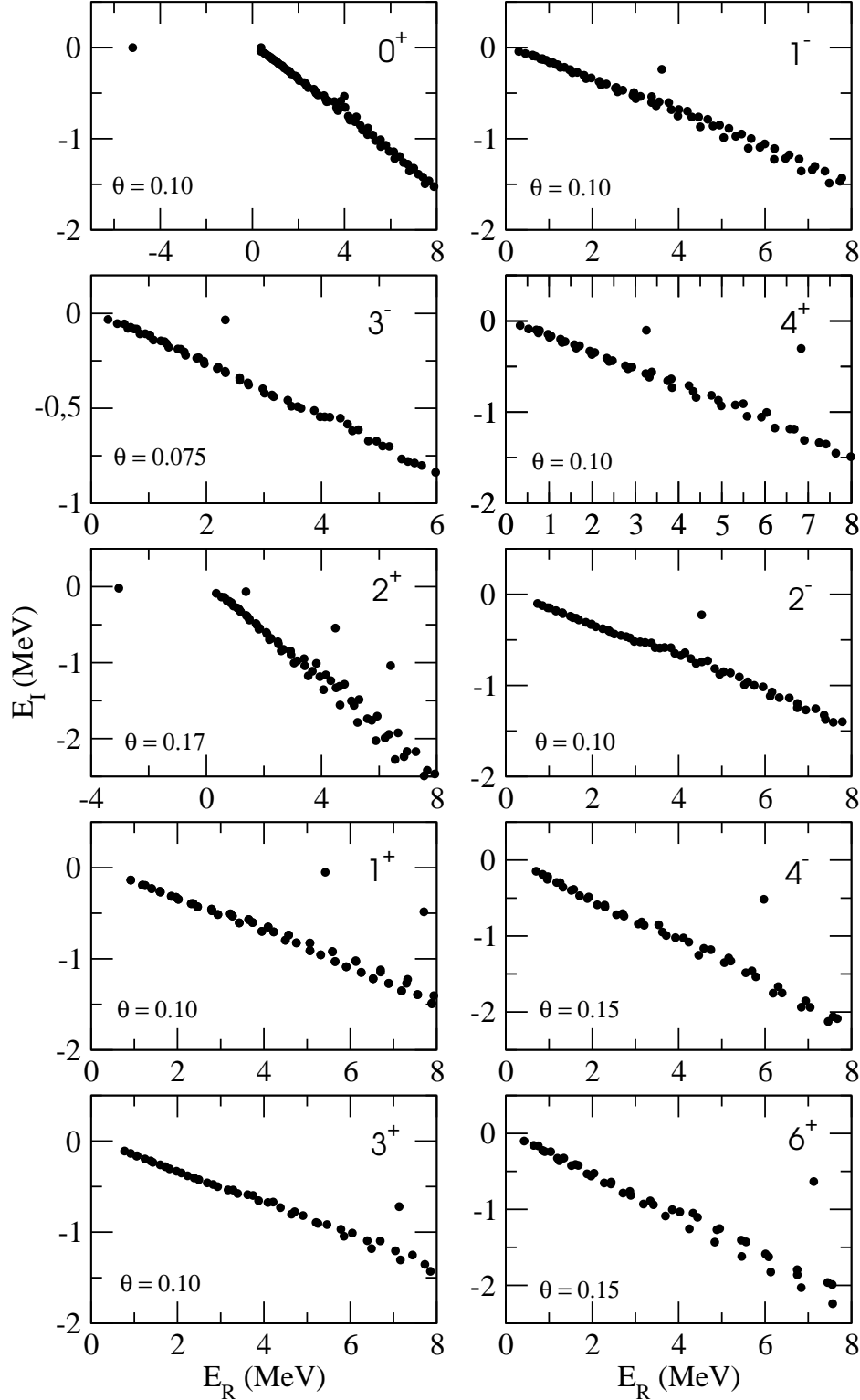


**Fig. 2.** The real ( $E_R$ ) and imaginary ( $E_I = -\Gamma/2$ ) parts of the energies for  $J^\pi$ -resonances in  $^{12}\text{C}$  obtained after complex rotation by the angle  $\theta$  also given in the figure. The two and three body interactions are specified in fig. 1.

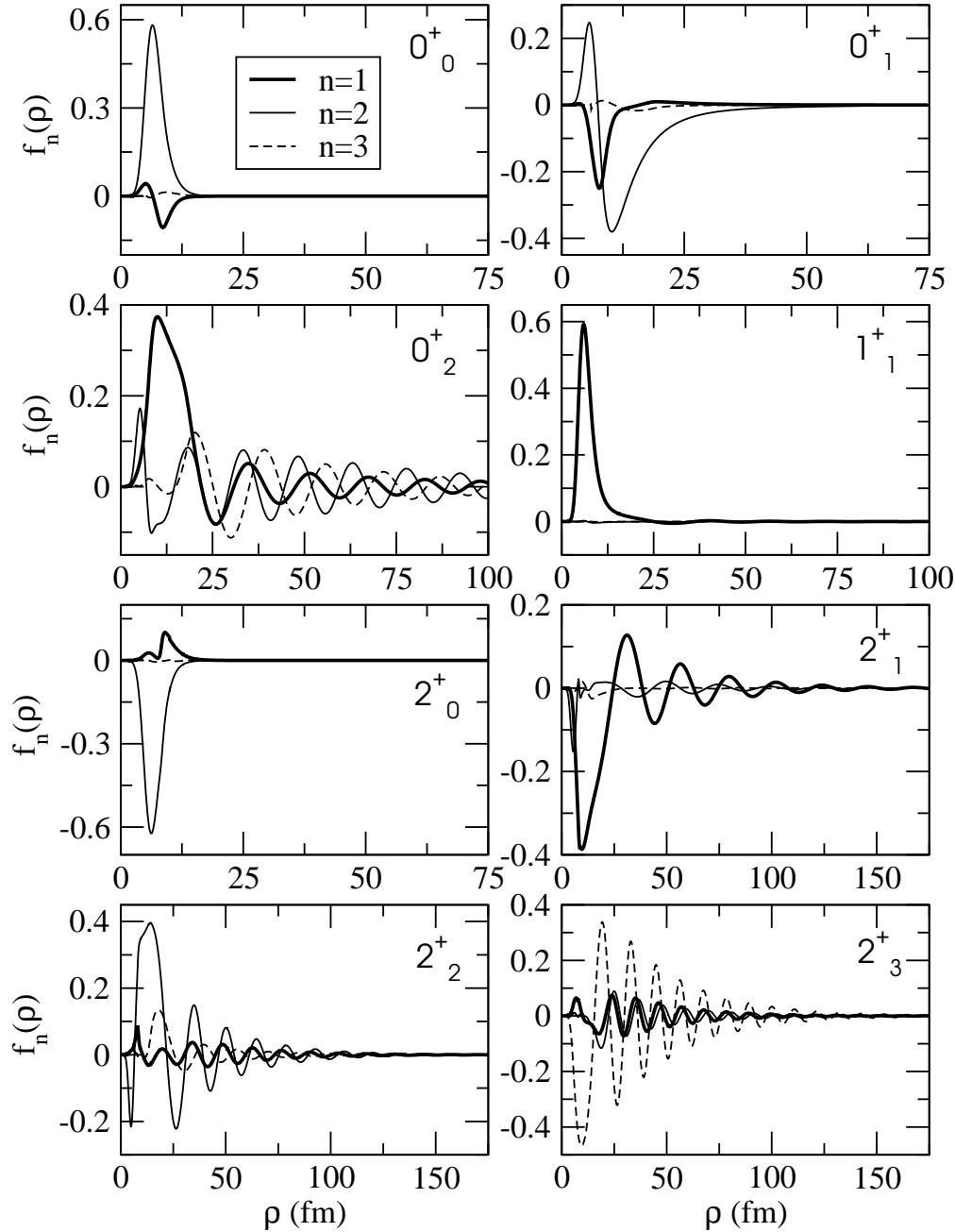


**Fig. 3.** The real parts of the three lowest adiabatic radial wavefunctions as functions of  $\rho$  for the  $0^+$ ,  $1^+$  and  $2^+$ -states of  $^{12}\text{C}$ . Their normalization reflects their relative contribution to each resonance. The two and three-body interactions are specified in fig. 1.

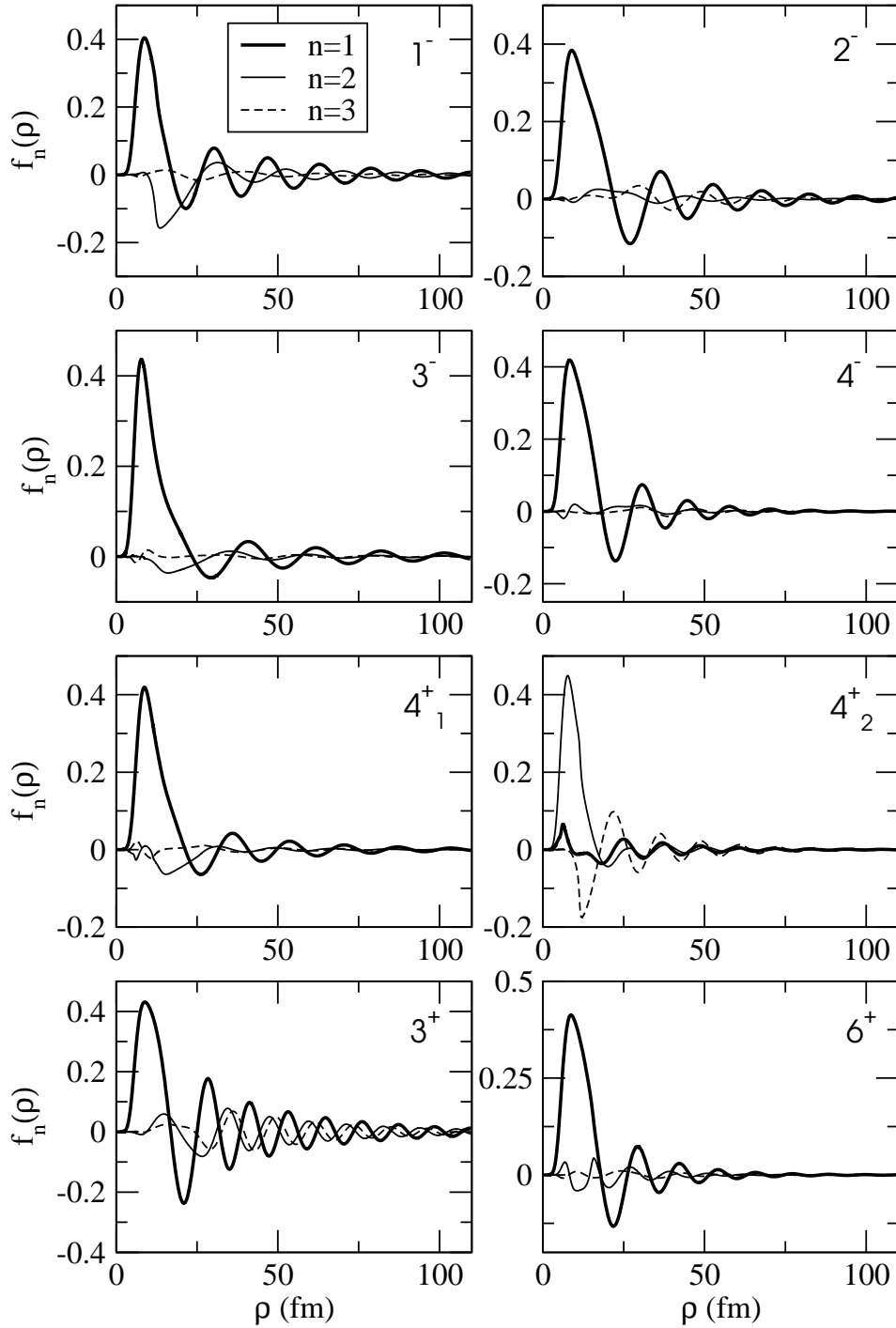
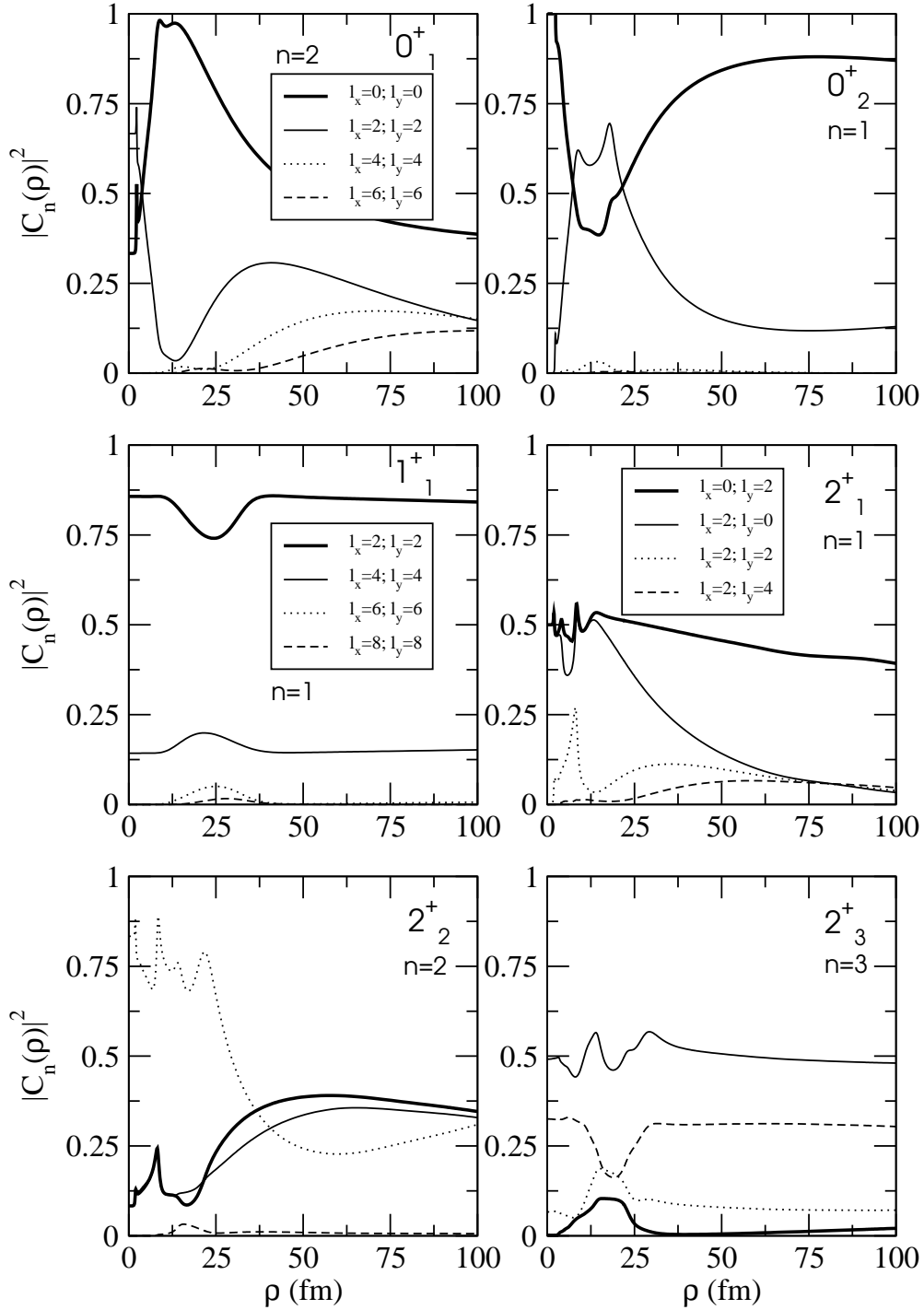
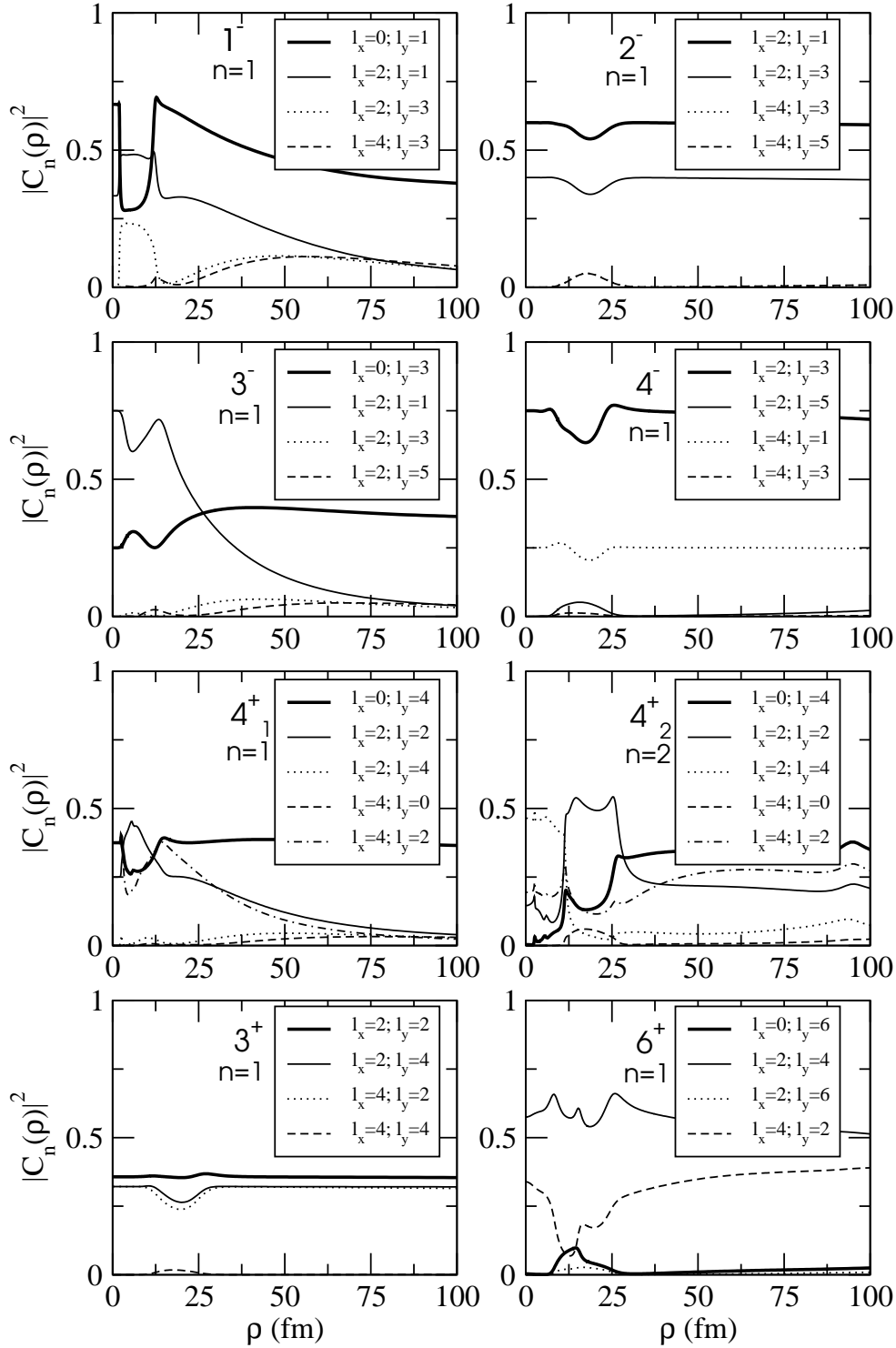


Fig. 4. The same as fig. 3 but for the  $1^-$ ,  $2^-$ ,  $3^-$ ,  $4^-$ ,  $4^+$ ,  $3^+$  and  $6^+$ -states of  $^{12}\text{C}$ .



**Fig. 5.** The partial wave decomposition of the  $^{12}\text{C}$  resonances with  $J^\pi$  as indicated on the figure shown as function of  $\rho$  for the dominating adiabatic eigenvalue. The two and three-body interactions are specified in fig. 1.



**Fig. 6.** The partial wave decomposition of the  $^{12}\text{C}$  resonances with  $J^\pi$  as indicated on the figure shown as function of  $\rho$  for the dominating adiabatic eigenvalue. The two and three-body interactions are specified in fig. 1.

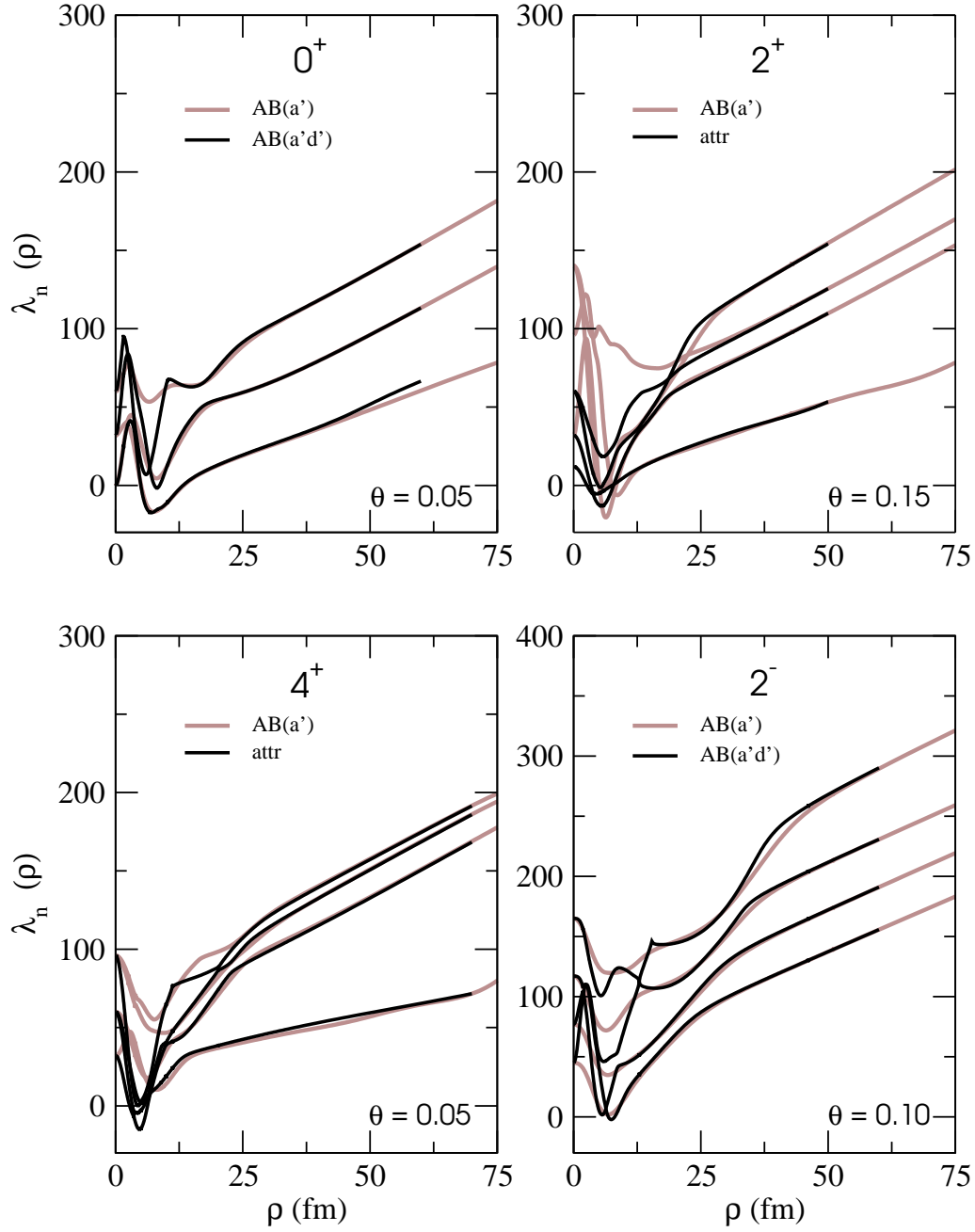


**Fig. 7.** The angular eigenvalues for some of the three-body resonances of  $^{12}\text{C}$  for different interactions. For the  $0^+$  and  $2^-$  three-body resonances we use “AB(a’)” and “AB(a’d’)”, whereas we use “AB(a’)” and “attr” for the  $2^+$  and  $4^+$ , see text for specifications.

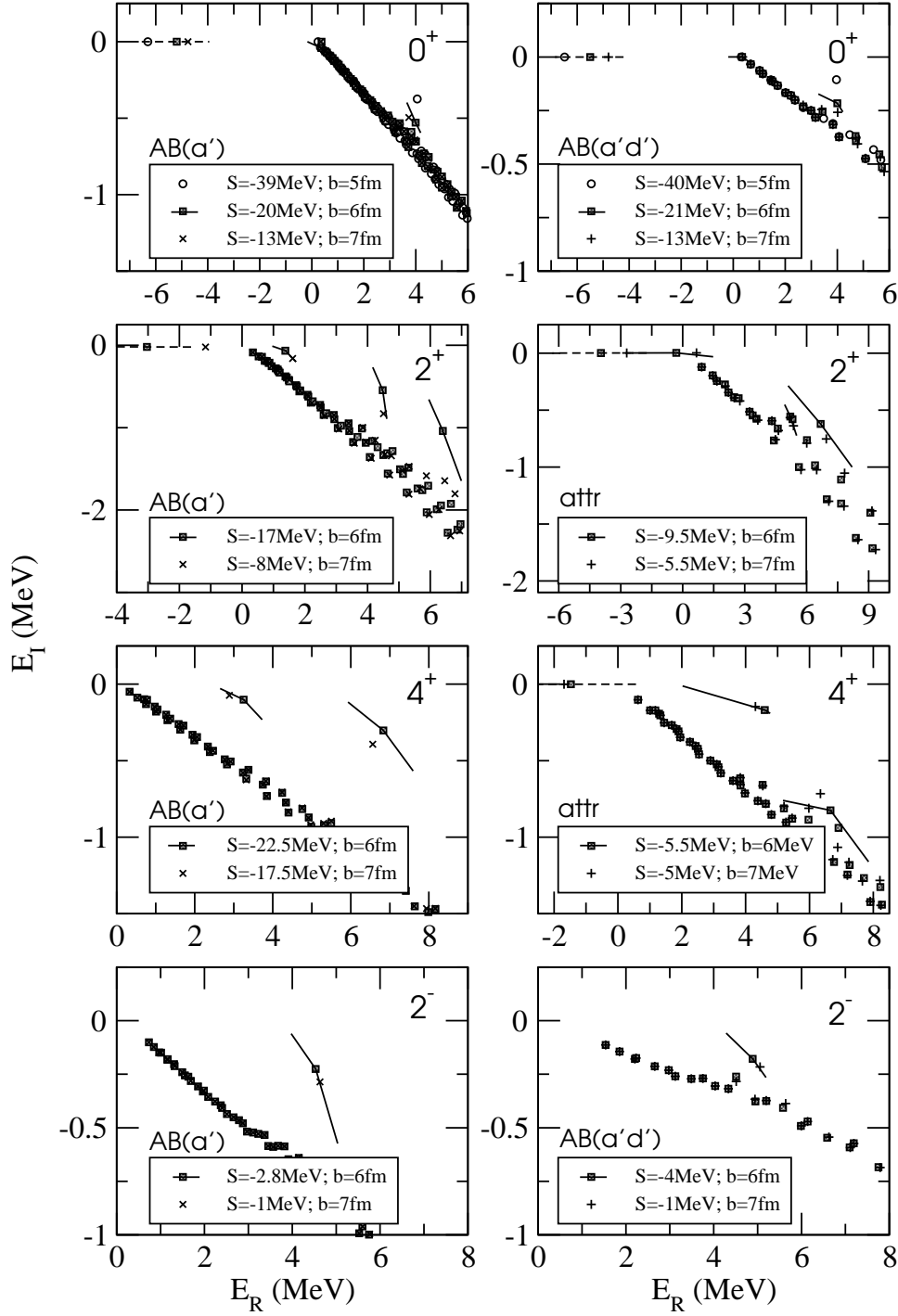


**Fig. 8.** The real and imaginary parts of the resonance energies for the four cases shown in fig. 7 obtained after rotation by the angle  $\theta$  for different two-body interactions. The left column is for the two-body interactions “AB(a’)” specified in fig. 1. The right column uses “AB(a’d’)” for  $0^+$  and  $2^-$ . The three-body interactions specified by strength and range are given in the figures. The lines are the resonance positions followed for  $b = 6$  fm when  $S$  is varied 5 MeV up or down from the central value.

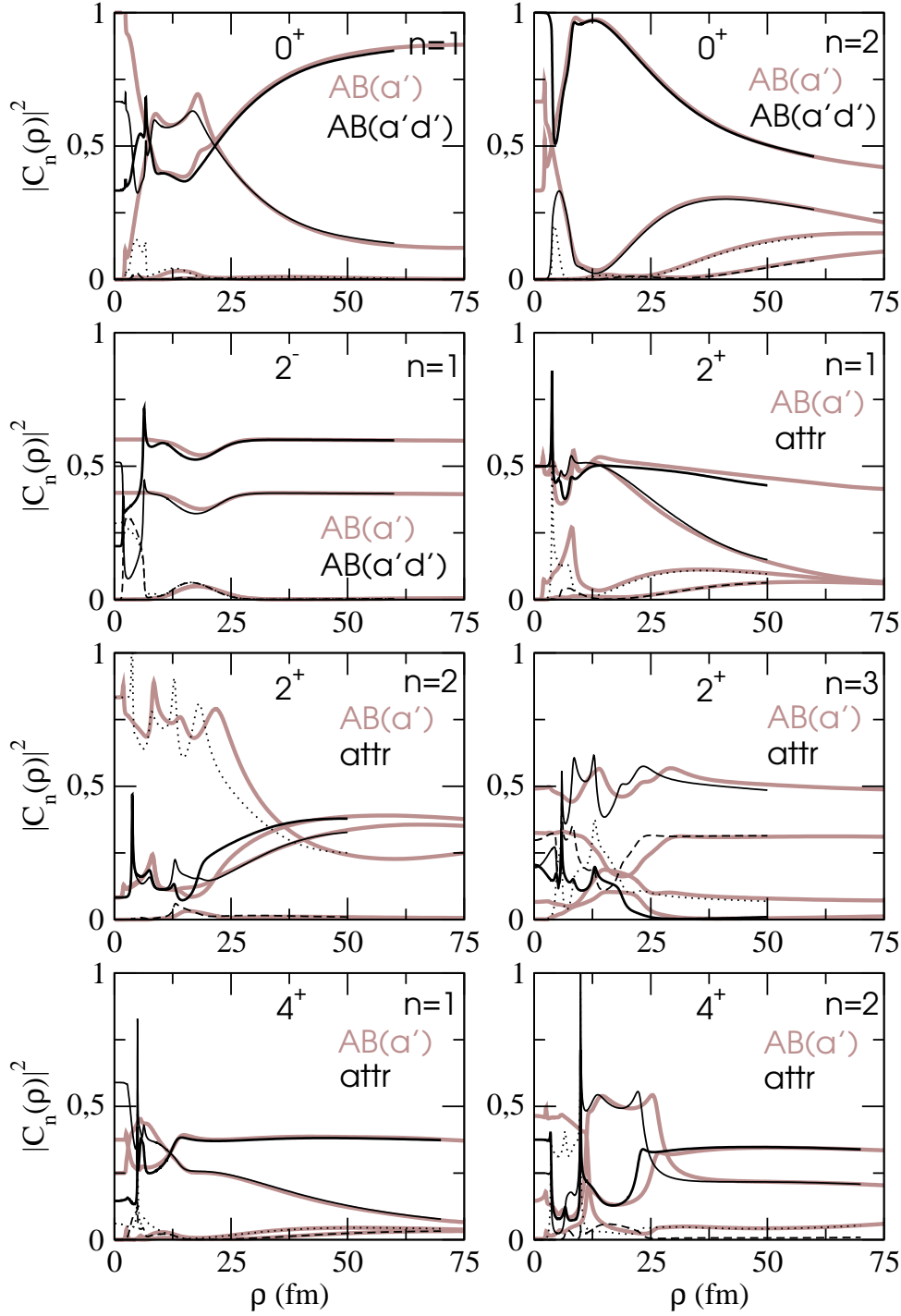


**Fig. 9.** The partial wave decomposition of the same  $^{12}\text{C}$  resonances for the two-body interactions given in the figures.

